

---

# A Hypernetwork-Based Approach to KAN Representation of Audio Signals

---

Patryk Marszałek<sup>\*1</sup> Maciej Rut<sup>\*1</sup> Piotr Kawa<sup>2</sup> Piotr Syga<sup>2</sup>

## Abstract

Implicit neural representations (INR) have gained prominence for efficiently encoding multimedia data, yet their applications in audio signals remain limited. This study introduces the Kolmogorov-Arnold Network (KAN), a novel architecture using learnable activation functions, as an effective INR model for audio representation. KAN demonstrates superior perceptual performance over previous INRs, achieving the lowest Log-Spectral Distance of 1.29 and the highest Perceptual Evaluation of Speech Quality of 3.57 for 1.5 s audio. To extend KAN’s utility, we propose FewSound<sup>1</sup>, a hypernetwork-based architecture that enhances INR parameter updates. FewSound outperforms the state-of-the-art HyperSound, with a 33.3% improvement in MSE and 60.87% in SI-SNR. These results show KAN as a robust and adaptable audio representation with the potential for scalability and integration into various hypernetwork frameworks.

## 1. Introduction

Implicit neural representations (INRs) represent discrete data in neural network weights. INR finds many applications in the case of image (Klocek et al., 2019), video (Chen et al., 2022), or 3D objects (Spurek et al., 2020). In the case of sound, INRs are unexplored, and only a few approaches are dedicated to such data. HyperSound (Szatkowski et al., 2023) presents an autoencoder-based architecture that takes on raw input sound and produces weight for INR-based sound representation. INRAS (Su et al., 2022) is an INR network that, by mapping the scene coordinates to the corresponding impulse responses, enables the modeling of spatial audio of interior scenes. Siamese SIREN (Lanzendörfer & Wattenhofer, 2023), is the extension of SIREN (Sitzmann et al., 2020) used for audio compression.

<sup>\*</sup>Equal contribution <sup>1</sup>Jagiellonian University, Kraków  
<sup>2</sup>Wrocław University of Science and Technology. Correspondence to: Patryk Marszałek <patryk.marszalek@student.uj.edu.pl>.

<sup>1</sup>The source code can be accessed at <https://github.com/gmum/fewsound.git>

The recently proposed KAN (Kolmogorov-Arnold Network) (Liu et al., 2024a) replaces traditional fully connected layers with activation functions. While KAN shows potential, it faces limitations with high-dimensional data. However, its effectiveness in low-dimensional settings and successful application to complex function regression tasks make it a promising candidate for audio INR.

This paper demonstrates that KAN is effective in modeling individual audio signals and can be extended to various functions through the hypernetwork paradigm. For single audio INR, KAN trains more rapidly and achieves better results. Setting up the conditions for a KAN is not immediately straightforward. We show that hypernetworks can generate KANs. In practice, we can directly produce KAN parameters or use updates for the universal KAN-based architecture. Therefore, we propose two methods. The first is a classical HyperSound (Szatkowski et al., 2023) with a KAN target network. The second uses a few-shot setting (Tancik et al., 2021; Batorski et al., 2024) in INR, which is an implementation of the Model-Agnostic Meta-Learning algorithm (MAML) (Finn et al., 2017). Since in a few-shot approach, there does not exist a model dedicated to audio signals, we introduce FewSound. FewSound takes raw sound on input and uses hypernetwork to generate updates to universal weights of INR dedicated to encoding sound. In our work, we examine six approaches: SIREN (Sitzmann et al., 2020), NeRF (Mildenhall et al., 2020), Random Fourier Features (Tancik et al., 2020), WIRE (Saragam et al., 2023), FINER (Liu et al., 2024b) and KAN (Liu et al., 2024a). In the model, we simultaneously train the hypernetwork weights and the universal weights. Thus, two settings show that KAN can be effectively modeled by hypernetworks.

Our study demonstrates that KAN model can be viewed as INR of sound. Such models yield favorable outcomes when dealing with individual audio signals and excel in large Hypernetwork-based models trained on large datasets.

Key contributions of our research include:

- showing KAN’s efficacy for continuous sound representation,
- comparing KAN representation with other INRs,

- showing that KAN can be produced via hypernetworks,
- introducing FewSound, a hypernetwork-based meta-learning method, which is used with KAN network and improves over previous hypernetwork approach HyperSound (Szatkowski et al., 2023),
- analysis of the parameters’s influence on the efficacy of the proposed method.

## 2. Related Work

To our knowledge, there are no specialized INR architectures focused on sound. Research papers on INR (Sitzmann et al., 2020; Tancik et al., 2020; Saragadam et al., 2023; Liu et al., 2024b; Müller et al., 2022) typically evaluate models using images, videos, and 3D objects as benchmarks. Although experiments involving sounds do exist, they remain relatively unexplored. In this section, we show that KAN effectively models single-audio in an efficient manner.

**INR** Implicit neural representations (INR) are data approximations based on neural networks relying on coordinate inputs. They enable discrete information such as pixels (Klocek et al., 2019; Chen et al., 2022), cloud points (Spurek et al., 2020), or audio magnitude information (Szatkowski et al., 2023) to be represented as continuous functions. The separation of the representation from spatial resolution makes the representation more memory efficient. Such information is limited by the networks’ architecture instead of the grid resolution. INRs are used in many signal processing problems, including 3D reconstruction (Mildenhall et al., 2020), super-resolution (Chen et al., 2022), compression (Strümpfer et al., 2022; Lanzendörfer & Wattenhofer, 2023) or audio scene representation (Su et al., 2022).

Initially, the INRs used ReLU-based MLPs. However, due to the ReLU’s second derivative being zero, they cannot capture the fine details of the information located in higher-order derivatives leading to worse performance. To counteract this, methods such as SIREN (Sitzmann et al., 2020) have been developed, which use a periodic activation function the sine in place of ReLU. The  $i$ -th layer of the network is defined as:  $\phi_i(x_i) = \sin(\omega_i W_i^T x_i + b_i)$ , where  $x_i$  is layer’s input, while  $W_i$  and  $b_i$  are, respectively, weights and biases. The use of the sine function enables SIREN to capture the details of the processed signals to a much greater degree than the widely used activation functions. Another example of a network architecture using a specialized activation function is WIRE (wavelet implicit neural representation) (Saragadam et al., 2023). Inspired by harmonic analysis, WIRE uses complex Gabor wavelet  $\psi$  as its nonlinearity activation:  $\psi(x) = e^{i\omega_0 x} e^{-|s_0 x|^2}$ .

INRs can suffer from a phenomenon called *spectral bias* (Rahaman et al., 2019) – the preference of MLPs to learn

low-frequency functions and ignore high-frequency noise, which can lead to performance degradation when high-frequency components of the input carry meaningful information (Gorji et al., 2023). A common way to overcome spectral bias is by introducing high-frequency embeddings (Mildenhall et al., 2020; Tancik et al., 2020) that modify the space over which the MLP operates, altering the frequency of its output function. FINER (Liu et al., 2024b) is an MLP-based architecture designed to flexibly tune the spectral bias. It uses a variable-periodic activation  $a(x) = \sin(\omega_0 |x+1|/x)$  and a specialized bias initialization schema in its first layer.

NERF (Neural Radiance Field) (Mildenhall et al., 2020) is a type of network originally designed for scene representation. Based on the 5D input of spatial location  $(x, y, z)$  and viewing direction  $(\theta, \phi)$ , the MLP network outputs color  $c = (r, g, b)$  and volume density  $(\sigma)$ . This allows the generation of 3D reconstructions of scenes from a set of sparse views.

**Sound representation** The audio encoders we rely on are classified into two main types: neural speech codecs and those employed in automatic speech recognition (ASR) or ASR-adjacent solutions.

SoundStream (Zeghidour et al., 2021) is a popular neural audio codec based on the encoder-decoder architecture. In our experiments we used only the encoder part composed of 1D convolution followed by four encoder blocks with residual units and the final 1D convolution.

SNAC (Siuzdak, 2024) uses the encoder based on the hierarchical tokens like the previous approach. The distinction is that the coarse tokens are sampled less frequently, resulting in covering broader time windows. SNAC not only decreases the bitrate required for reconstruction, but also provides useful information in language modeling tasks.

Whisper (Radford et al., 2023) is a Transformer-based (Vaswani et al., 2017) ASR system, trained on 680,000 hours of data, achieving state-of-the-art speech recognition results. It was successfully adapted to various other tasks including audio-language models (Chu et al., 2023), voice conversion (Guo et al., 2023), text-to-speech (Collabora, 2024) and audio DeepFake detection (Kawa et al., 2023). In our experiments, we use only Whisper’s encoder.

Spectrogram Encoder is based on VoiceBlock (O’Reilly et al., 2022) — originally developed as a speech-to-speech solution for adversarial examples against ASR models. The encoder is based on the linear-spectrogram input that extracts a feature vector composed of fundamental frequency, aperiodicity and loudness of the signal.

**KAN (Kolmogorov-Arnold Network)** KANs (Liu et al., 2024a) is a type of neural network architecture used as an

alternative to MLPs, instead of using fixed activation functions. KANs utilize learnable activation functions placed on edges rather than nodes. KAN’s learnable functions are parametrized as a spline and serve as ”weights”, whereas the nodes only sum the incoming signals. This is described by the following formula:

$$f(x) = \sum_{q=1}^{2n+1} \Phi_q \left( \sum_{p=1}^n \phi_{q,p}(x_p) \right),$$

where  $\Phi_q$  is a KAN layer,  $\phi_{q,p}$  is a single activation function and  $x_p$  is input feature. The authors also introduced an architecture of LANs (learnable activation networks) – the only difference between them and MLP lies in the learning aspect of the activation functions. The authors show that a network can be used in implicit neural representation tasks.

**Audio INR** In the realm of acoustic data, INR transforms a one-dimensional temporal space into the corresponding amplitude values. Therefore, our INR is depicted as:

$$f_\theta : \mathbb{R} \rightarrow \mathbb{R},$$

where  $f_\theta(t)$  denotes the amplitude of the sound over time.

We consider six variants of INRs: NeRF, SIREN, RFF, FINER, WIRE and KAN. We use NeRF to refer to a network with positional encoding, followed by a MLP with ReLU activation. The positional encoding, described by  $\gamma(t) = [\sin(2^0\pi t), \cos(2^0\pi t), \dots, \sin(2^{L-1}\pi t), \cos(2^{L-1}\pi t)]$  is taken from the original NeRF (Mildenhall et al., 2020).

SIREN (Sitzmann et al., 2020) is a MLP with sine activation:  $a(x) = \sin(\omega_0 x)$ , where  $\omega_0$  is a hyperparameter.

RFF (Random Fourier Features) (Tancik et al., 2020) is used to refer to a multilayer perceptron with ReLU activation and input embedding defined as  $\gamma(t) = [\cos(2\pi \mathbf{B}t), \sin(2\pi \mathbf{B}t)]$ , where  $\mathbf{B} \in \mathbb{R}^{m \times d}$  is a random projection matrix, sampled from  $\mathcal{N}(0, \sigma^2)$ . In our case  $d$ , the dimensionality of the input, is always equal to 1, while  $\sigma$  and  $m$  are hyperparameters.

WIRE (Saragadam et al., 2023) is a MLP with complex Gabor wavelet activation  $a(x) = e^{i\omega_0 x} e^{-|s_0 x|^2}$ , where  $\omega_0$  and  $s_0$  are hyperparameters.

FINER (Liu et al., 2024b) is a MLP with activation function defined as  $a(x) = \sin(\omega_0|x + 1|x)$ , where  $\omega_0$  is a hyperparameter. The bias of its first layer is initialized by sampling from  $\mathcal{U}(-k, k)$ , where  $k$  is a hyperparameter.

Our Kolmogorov-Arnold network implementation consists of the same positional encoding as in NeRF, followed by KAN layers. Each KAN layer can be described by  $\phi(x) = w_b \text{SiLU}(x) + w_s \text{spline}(x)$ , where  $w_b$  and  $w_s$  are matrices of learnable weights, and  $\text{spline}(x)$  is a linear combination of B-splines such that  $\text{spline}(x) = \sum_i c_i B_i(x)$ ,

with learnable  $c_i$ s. It is parametrized by *spline order* – the degree of the used spline, and *grid size* – the number of knots defining the spline.

### 3. KAN in hypernetwork-based architectures

In this section, we show how KAN works with hypernetworks. We use two main approaches. First, we use the autoencoder-based solution HyperSound (Szatkowski et al., 2023), where we add KAN as the target model. We also examine KAN in a few-shot setting introduced by (Wang et al., 2020). To examine such a model, we propose FewSound, which is a realization of (Wang et al., 2020) in the case of KAN and hypernetworks.

**Hypernetwork** In the foundational study (Ha et al., 2016) hyper-networks are described as neural models that produce weights for another network tasked with solving a specific problem. The researchers aim to decrease the number of trainable parameters by creating a hyper-network with fewer parameters than the target network. Drawing a parallel between hypernetworks and generative models, the authors of (Sheikh et al., 2017) employ this technique to generate a variety of target networks that approximate the same function.

**Few-shot learning for INR** A significant limitation of deep learning models is their reliance on extensive datasets. In contrast, humans can learn effectively from just a few examples. A few-shot learning (Wang et al., 2020) approach was proposed to bridge the gap between deep neural network training and human learning capabilities. This strategy treats the data set as consisting of numerous small tasks. Few-shot architectures can be quickly adapted to solve new problems in a single step. The most popular approach to few-shot learning is MAML (Finn et al., 2017). MAML uses a set of universal weights, fine-tuned for specific small tasks through a limited number of gradient updates. Due to the model-agnostic nature of the approach, it can be adapted to various models and corresponding learning algorithms.

The terminology of few-shot learning is often inconsistent due to varying definitions in existing research. For a standardized framework (Chen et al., 2019; Wang et al., 2020). However, such a nomenclature is dedicated to a classification, regression, or generative model task. In the case of the INR-based model, we refer to (Tancik et al., 2021). We have a data set  $X$  that contains sound samples, and our goal is to produce INR  $f_\theta$  that encodes sound in network weights.

**FewSound** Now we are ready to present FewSound – a model that uses Hypernetworks to update the INR weights dedicated to sound. The core concept of this update mechanism is to use information extracted from raw sound data and universal weights to determine the optimal updates for

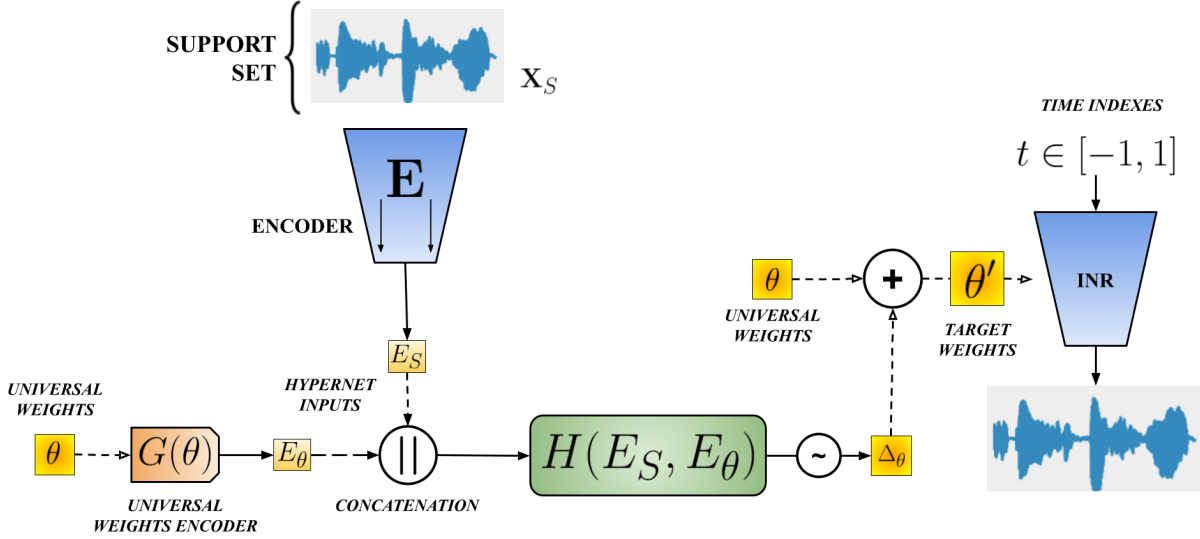


Figure 1: The overview of FewSound architecture. The input row sound is processed by encoding network  $E(\cdot)$  and delivered to the fully connected Hypernetwork  $H(\cdot)$  together universal weights. The Hypernetwork transforms them and returns the update of weights  $\Delta\theta$  for the target INR  $f_{\theta'}$ . The target network  $f_{\theta'}$  transforms time samples into the amplitude of the sound, dedicated to the considered task.

Table 1: Reconstruction metrics for 1.5 s and 3 s audio. We report mean and standard deviation across 110 samples, each of a different speaker of VCTK dataset (Veaux et al., 2013).

1.5 s audio							
INR (# params)	MSE $\rightarrow 0$	PSNR $\rightarrow \infty$	LSD $\rightarrow 0$	SI-SNR $\rightarrow 100$	PESQ $\rightarrow 4.5$	STOI $\rightarrow 1$	CDPAM $\rightarrow 0$
<i>NERF</i> (33,261)	$8.1e-4 \pm 1.3e-3$	$39.68 \pm 5.67$	$1.36 \pm 0.18$	$17.83 \pm 6.10$	$3.21 \pm 0.48$	$0.98 \pm 0.04$	$0.25 \pm 0.11$
<i>SIREN</i> (31,191)	$4.4e-4 \pm 4.9e-4$	$40.82 \pm 3.68$	$1.40 \pm 0.26$	$19.71 \pm 2.67$	$2.76 \pm 0.43$	$0.95 \pm 0.06$	$0.23 \pm 0.14$
<i>FINER</i> (31,191)	$1.9e-4 \pm 2.3e-4$	$44.39 \pm 3.61$	$2.06 \pm 0.27$	$23.29 \pm 4.29$	$2.26 \pm 0.29$	$0.93 \pm 0.08$	$0.51 \pm 0.11$
<i>WIRE</i> (31,191)	$4.8e-4 \pm 6.5e-4$	$41.91 \pm 5.53$	$1.63 \pm 0.25$	$20.77 \pm 5.91$	$2.79 \pm 0.44$	$0.96 \pm 0.05$	$0.16 \pm 0.08$
<i>RFF</i> (39,201)	$8.7e-4 \pm 8.8e-4$	$38.63 \pm 4.93$	$1.56 \pm 0.16$	$17.81 \pm 5.58$	$2.94 \pm 0.39$	$0.98 \pm 0.01$	$0.19 \pm 0.09$
<b>KAN</b> (33,768)	$6.7e-4 \pm 2e-3$	$42.44 \pm 6.72$	$1.29 \pm 0.22$	$20.50 \pm 6.94$	$3.57 \pm 0.42$	$0.99 \pm 0.02$	$0.13 \pm 0.08$
3 s audio							
INR (# params)	MSE $\rightarrow 0$	PSNR $\rightarrow \infty$	LSD $\rightarrow 0$	SI-SNR $\rightarrow 100$	PESQ $\rightarrow 4.5$	STOI $\rightarrow 1$	CDPAM $\rightarrow 0$
<i>NERF</i> (33,261)	$4.6e-4 \pm 5.0e-4$	$40.83 \pm 4.50$	$1.47 \pm 0.16$	$17.54 \pm 4.29$	$2.54 \pm 0.45$	$0.94 \pm 0.05$	$0.30 \pm 0.14$
<i>SIREN</i> (31,191)	$5.3e-4 \pm 3.6e-4$	$39.20 \pm 3.35$	$1.42 \pm 0.18$	$14.41 \pm 4.44$	$2.25 \pm 0.28$	$0.96 \pm 0.03$	$0.41 \pm 0.14$
<i>FINER</i> (31,191)	$1.9e-4 \pm 1.8e-4$	$43.77 \pm 3.19$	$2.21 \pm 0.16$	$19.05 \pm 3.51$	$1.89 \pm 0.25$	$0.95 \pm 0.07$	$0.45 \pm 0.12$
<i>WIRE</i> (31,191)	$4.3e-4 \pm 3.9e-4$	$40.30 \pm 3.42$	$1.52 \pm 0.10$	$15.45 \pm 4.36$	$2.33 \pm 0.35$	$0.95 \pm 0.07$	$0.33 \pm 0.13$
<i>RFF</i> (39,201)	$5.3e-4 \pm 3.6e-4$	$39.20 \pm 3.35$	$1.42 \pm 0.18$	$14.41 \pm 4.44$	$2.25 \pm 0.28$	$0.96 \pm 0.03$	$0.40 \pm 0.14$
<b>KAN</b> (33,768)	$3.8e-4 \pm 4.4e-4$	$42.28 \pm 5.31$	$1.34 \pm 0.19$	$18.85 \pm 5.08$	$2.89 \pm 0.51$	$0.97 \pm 0.03$	$0.33 \pm 0.15$



a particular task. This method adjusts the INR’s parameters for entirely different sounds.

The schema of FewSound is provided in Fig. 1. We aim to reconstruct the training example using the target network. In practice, we run our INR on all steps to reconstruct the input.

Following our previous analysis of INR in the sound reconstruction task, we consider the parameterized function  $f_\theta$  to be one of the discussed INRs. In addition, we distinguish the trainable encoding network  $E(\cdot)$  in our architecture, which transforms raw audio data into low-dimensional representation. We investigated various encoder architectures and report their performance in Tab. 5.

The encoded sound is concatenated with universal weights propagated by the universal weight encoder  $\mathbf{G}(\cdot)$  and then to the fully connected hypernetwork  $H(\cdot)$ . The hypernetwork then modifies the universal weights:  $\theta' = \theta + \Delta_\theta$ . In contrast to the traditional MAML approach, which uses a gradient-based adaptation step, we propose employing a Hypernetwork to anticipate the values directly from the data.

The parameters for the final target model are calculated with the formula in Eq. 1.

$$\theta' = \theta + \Delta_\theta = \theta + H(\mathbf{E}_S, \mathbf{E}_\theta). \quad (1)$$

**Training** For training the model, we assume that the encoder  $E(\cdot)$  is parametrized by  $\gamma$ ,  $E := E_\gamma$ . The universal weight encoder  $G(\cdot)$  is parameterized by  $\delta$ , and the Hypernetwork  $H(\cdot)$  by  $\eta$ ,  $H := H_\eta$ . During training, we first sample the batch of sounds  $\mathcal{B}$  from the given dataset  $X$ . Next, for each task data, we calculate the update  $\Delta_\theta$ , using the hypernetwork and provide the updated parameters  $\theta'$  according to the rule given in (1). Finally, the objective to train the parameters of the system is calculated using the timesteps from  $[-1, 1]$ :

$$\mathcal{L}_{HyperMAML}(f_\theta) = \sum_{\mathcal{T}_i \in \mathcal{B}} \mathcal{L}_{Q_i}(f_{\theta'}) = \sum_{\mathcal{T}_i \in \mathcal{B}} \mathcal{L}_{Q_i}(f_{\theta + \Delta_\theta}), \quad (2)$$

where  $\mathcal{L}_{Q_i}(f_{\theta'}) = \lambda_t L_t(x, \hat{x}) + \lambda_f L_f(x, \hat{x})$ , with  $L_t$  is L1 loss in temporal space,  $L_f$  is multi-resolution mel-scale STFT loss in frequency space (Yamamoto et al., 2020) and  $\lambda_s$  are coefficients controlling influence of particular losses. The Encoder parameters, universal weight encoder, Hypernetwork, and global parameters  $\theta$  represent the meta parameters of the system and are updated with stochastic gradient descent (SGD) by optimizing  $\mathcal{L}_{HyperMAML}(f_\theta)$ .

## 4. Experiments

In this section, we perform an experimental analysis. We divide it into two subsections: analysis of the performance

of different INR architectures and experimental results of our hypernetwork approach, FewSound.

Multiple metrics are used to evaluate the quality of reconstructions. That includes quantitative metrics such as MSE, Log-spectral distance (LSD), PSNR, and SI-SNR. We also use metrics that measure the perceptual quality of the audio signal, such as PESQ (Rix et al., 2001), STOI (Taal et al., 2010), and CDPAM (Manocha et al., 2021). Given that the perception of ‘natural’ sound is critical to our output, we prioritized the PESQ metric due to its strong correlation with human auditory perception.

### 4.1. Implicit Neural Representations

We compare the aforementioned INR architectures using two subsets of the VCTK (Veaux et al., 2013) dataset. Each of the subsets is generated by randomly choosing one recording per speaker, resampling it to 22.05 kHz and randomly cropping it to a desired length. We crop the recordings to 32,768 samples (about 1.5 seconds) in the first subset and to 65,536 (about 3 seconds) in the second subset. Both subsets consist of a total of 110 recordings. To make a fair comparison, all of the MLP based INRs have the same number of layers and the same sizes of layers, while KANs have their architecture chosen in a way that the number of parameters is similar to the other models. All architectures are trained for 10,000 steps, using the AdamW optimizer (Loshchilov & Hutter, 2019) and the same loss function as in FewSound. Table 1 shows the results of the experiments. All INRs were selected to be close in the number of parameters. One may note that, with the exception of MSE, the shorter audios result in better quality. KAN is competitive for most metrics, achieving the best mean score in LSD, PESQ, STOI and CDPAM and second best PSNR for 1.5 s audio; as well as the best mean LSD, PESQ, STOI, and second best MSE, PSNR, SI-SNR, CDPAM for 3 s audio.

### 4.2. Hypernetworks

**Setting** When using hypernetworks, we only consider NeRF, SIREN, and KAN as the target network architectures. We compare our method with the state-of-the-art model HyperSound (Szatkowski et al., 2023) and follow the same experimental setting. We use the VCTK dataset resampled to 22,050 Hz. The inputs have a length of 32,768 samples and are obtained by cropping the original recordings. The last 10 speakers are used as the validation set. All models are trained for 2,500 epochs, with 10,000 training samples chosen randomly for each epoch. We use AdamW optimizer (Loshchilov & Hutter, 2019) and OneCycleLR scheduler (Smith & Topin, 2018). The initial learning rate is set to  $1e-5$ , with the exception of runs using the SIREN target network, where it is set to  $1e-6$ .

We examine how different encoder and target network archi-

tures impact the quality of reconstructions. In particular, we explore the performance of KAN-based target networks used both with FewSound and HyperSound models.

Unless otherwise mentioned, FewSound uses a SoundStream (Zeghidour et al., 2021) based encoder, 17.5M parameter hypernetwork MLP and NERF-based target network. The number of parameters in target networks is roughly equal to the length of the input audio (32K). Results for HyperSound are taken from the original paper.

**Results** Table 2 shows the comparison of our model with state-of-the-art HyperSound. We include results for two sizes of the hypernetwork MLP – a smaller 17.5M parameter model and a larger one with 41.2M parameters. Both of them have comparable results, showing that the smaller network may be used for efficiency. One may note that even the smaller one outperforms HyperSound in all the metrics (MSE by 33.3%, LSD by 6.83%, SI-SINR by 60.87%, PESQ by 8.66%, STOI by 2.63% and CDPAM by 13.89%).

Table 2: FewSound performance compared to HyperSound.

Model	MSE → 0	LSD → 0	SI-SNR → 100	PESQ → 4.5	STOI → 1	CDPAM → 0
HyperSound	0.009	1.61	2.99	1.27	0.76	0.36
FewSound 17.5M	<b>0.006</b>	<b>1.50</b>	4.81	1.38	0.78	0.31
FewSound 41.2M	<b>0.006</b>	<b>1.50</b>	<b>5.03</b>	<b>1.41</b>	<b>0.79</b>	<b>0.30</b>

**Impact of target network architecture** Tables 3 and 4 show how different target network architectures impact the quality of reconstructions using FewSound and HyperSound models, respectively. Note that for FewSound NERF outperforms other architectures in terms of all metrics, with KAN close second (between 1.1% and 16% worse). Whereas, for HyperSound, KAN is better in 4 out of 6 metrics (between 1.3% and 28.5%) and worse in two (0.6% and 11%). For all the experiments, SIREN performs the worst.

Table 3: Performance of FewSound with different target network architectures.

	MSE → 0	PSNR → ∞	LSD → 0	SI-SNR → 100	PESQ → 4.5	STOI → 1	CDPAM → 0
NERF	<b>0.006</b>	<b>28.07</b>	<b>1.50</b>	<b>4.81</b>	<b>1.38</b>	<b>0.78</b>	<b>0.31</b>
KAN	0.007	27.76	1.55	4.26	1.36	0.77	0.36
SIREN	0.025	22.02	1.74	-9.40	1.18	0.64	0.31

**Ablation Study** Table 5 shows the impact of using different encoder architectures, mentioned in Section 2. SoundStream, SNAC, and Spectrogram Encoder were trained from scratch. In the case of Whisper, we base on the pre-trained

Table 4: Performance of HyperSound with different target network architectures. Results for SIREN and NERF are taken from the original paper, while we train the model using the KAN target network architecture ourselves. A target network with a significantly lower number of parameters (19K) is used in this case, as it achieves better results.

	MSE → 0	LSD → 0	SI-SNR → 100	PESQ → 4.5	STOI → 1	CDPAM → 0
NERF	0.009	<b>1.61</b>	2.99	1.27	0.76	<b>0.36</b>
KAN	<b>0.007</b>	1.62	<b>3.98</b>	<b>1.29</b>	<b>0.77</b>	0.40
SIREN	0.018	3.56	-3.66	1.19	0.65	0.3

checkpoints - *tiny.en* and *large-v2* and finetune using the LoRA approach (Hu et al., 2022).

Table 5: FewSound performance with different encoder architectures.

Encoder	MSE → 0	PSNR → ∞	LSD → 0	SI-SNR → 100	PESQ → 4.5	STOI → 1	CDPAM → 0
SoundStream	<b>0.006</b>	<b>28.07</b>	1.50	<b>4.81</b>	1.38	0.78	0.31
Whisper L	0.042	19.72	1.40	-27.67	1.30	0.75	0.31
Whisper T	0.039	20.10	1.40	-29.08	1.25	0.72	0.33
Spectral	0.045	19.46	<b>1.35</b>	-21.76	<b>1.49</b>	<b>0.80</b>	<b>0.29</b>
SNAC	0.007	27.55	1.56	4.03	1.30	0.77	0.32

We further analyze the influence of various parameters’ values on the KAN’s performance. In the ablation study, experiments are also conducted on audio samples of 1.5 seconds and 3 seconds, with each subset limited to only 10 recordings. Due to the page limit, we include selected results for 1.5 s audio. More parameters and analysis of 3 s audio samples can be found in Appendix A. During our study we keep the following base parameters’ values, changing only the analyzed components: *encoding length* = 8, *grid size* = 10, *spline order* = 2, *layer sizes* = [48, 24, 12], *scale noise* = 0.1, *scale base* = 1, *scale spline* = 1, *learning rate* = 5e-3 and *enable scale spline* = True, which controls whether we include the learnable spline weights matrix  $w_s$ . Theoretically, these weights are redundant, as they could be absorbed into the spline itself.

Table 6 illustrates the impact of the length of the encoding (size of the positional encoding) that directly influences the size of networks. Values smaller than the baseline of 8 result in progressively worse performance; meanwhile, increasing the length provides improvement up to value of 16, where the results are the best for all but one metric (LSD).

Table 7 demonstrates the impact of different hidden layer configurations. The results indicate a consistent performance improvement as network capacity increases, with

Table 6: KAN performance on the 1.5 s samples, with respect to the encoding length. The results are averaged across 10 samples.

Enc. Len.	#Params	MSE	PSNR	LSD	SI-SNR	PESQ	STOI	CDPAM
		→ 0	→ ∞	→ 0	→ 100	→ 4.5	→ 1	→ 0
2	23,016	0.0033	30.7170	2.3927	9.0285	1.4980	0.7556	0.3731
4	25,704	0.0017	33.7562	1.6014	12.3093	1.9463	0.9040	0.2561
8	31,080	0.0007	40.0990	<b>1.2884</b>	18.9503	3.3588	0.9904	0.1913
10	33,768	0.0005	41.1152	1.3921	20.0078	3.4947	0.9930	0.1574
12	36,456	0.0005	42.6504	1.4182	21.6062	3.5176	0.9949	0.1664
16	41,832	<b>0.0002</b>	<b>46.8576</b>	1.4194	<b>25.9786</b>	<b>3.6256</b>	<b>0.9957</b>	<b>0.1538</b>
24	52,584	0.0003	45.7863	1.4764	24.9128	3.6033	0.9955	0.1982

Table 7: KAN results on 1.5 s samples in relation to different number and sizes of hidden layers.

Layer Sizes	#Params	MSE	PSNR	LSD	SI-SNR	PESQ	STOI	CDPAM
		→ 0	→ ∞	→ 0	→ 100	→ 4.5	→ 1	→ 0
[24, 12, 6]	10,500	0.0014	35.9192	1.4806	14.5340	2.1313	0.9360	0.2977
[24, 24, 12, 6]	18,564	0.0012	37.6839	1.3589	16.4163	2.7035	0.9778	0.2746
[48, 12, 6]	19,908	0.0010	38.5736	1.3589	17.3090	2.8569	0.9795	0.2679
[48, 12, 12, 6]	21,924	0.0010	38.2946	1.3557	17.0775	2.9597	0.9810	0.2618
[48, 16, 8]	23,408	0.0009	38.7324	1.3347	17.5094	3.0476	0.9845	0.2451
[48, 24, 12]	31,080	0.0007	40.0990	1.2884	18.9503	3.3588	0.9904	0.1913
[96, 48, 24]	102,480	<b>0.0003</b>	<b>43.6428</b>	<b>1.1715</b>	<b>22.5679</b>	<b>4.0203</b>	<b>0.9964</b>	<b>0.1072</b>

the architecture containing hidden layers of [96, 48, 24] achieving the best performance. Decreasing the networks size leads to progressive results degradation.

Table 8 presents a comparison of the varying spline order values (the degree of the applied spline). Increasing the spline order allows creation of more complex spline functions; however, this comes at the cost of additional parameters. In our study, an order of 3 provides the best overall performance across both quantitative (PSNR) and perceptual (PESQ) metrics. Using smaller or larger spline orders leads to a decline in metric scores.

Table 9 provides insights into the influence of grid size (number of knots defining the spline) on KAN’s learning process. Similarly to encoding length and spline order, an increase in grid size leads to a higher number of INR parameters. While a larger spline order eventually results in a decline in reconstruction quality, this effect is not observed with grid size. Extra parameters enhance the expressiveness of the INR, improving all metrics except LSD.

Table 8: KAN spline order (O) for 1.5 s audio recordings

O	Params	MSE	PSNR	LSD	SI-SNR	PESQ	STOI	CDPAM
		→ 0	→ ∞	→ 0	→ 100	→ 4.5	→ 1	→ 0
1	28,860	9e-4	38.83	1.53	17.59	3.01	0.98	0.27
2	31,080	<b>7e-4</b>	40.10	1.29	18.95	3.36	<b>0.99</b>	0.19
3	33,300	<b>7e-4</b>	<b>40.43</b>	1.23	<b>19.28</b>	<b>3.46</b>	<b>0.99</b>	<b>0.18</b>
5	37,740	1e-3	38.87	<b>1.22</b>	17.66	3.38	<b>0.99</b>	0.19
7	42,180	9e-4	38.91	1.23	17.71	3.21	0.98	0.21

Table 9: Impact of spline function grid size (G) on 1.5 s reconstructions

G	Params	MSE	PSNR	LSD	SI-SNR	PESQ	STOI	CDPAM
		→ 0	→ ∞	→ 0	→ 100	→ 4.5	→ 1	→ 0
1	11,100	3e-3	30.65	2.00	8.99	1.65	0.80	0.43
5	19,980	1e-3	37.33	1.36	16.01	2.61	0.97	0.27
10	31,080	7e-4	40.10	<b>1.29</b>	18.95	3.36	0.99	0.19
12	35,520	5e-4	42.34	1.30	21.24	3.65	0.99	0.16
17	46,620	<b>3e-4</b>	<b>44.78</b>	1.31	<b>23.78</b>	<b>3.81</b>	<b>1.00</b>	<b>0.13</b>

**Spectrograms** The spectrograms shown in Fig. 2 illustrate differences in the fidelity of sound reconstruction achieved by various INRs compared to the ground truth. Across all methods, the harmonic structures in the low-frequency range are generally well-preserved, reflecting their ability to capture fundamental features of the audio signal. However, significant variations emerge in the representation of high-frequency components, where most INRs lowers the intensity of the components. It is particularly visible with FINER. Moreover, all of the INRs (with KAN and NERF to the least degree) demonstrate a tendency to over-smooth the higher intensities in high-frequency components, which results in adding white noise. Finally, one can note the lower average intensity in the reconstructed audio.

## 5. Conclusion

This work demonstrates the effectiveness of Kolmogorov-Arnold Networks (KANs) as implicit neural representations

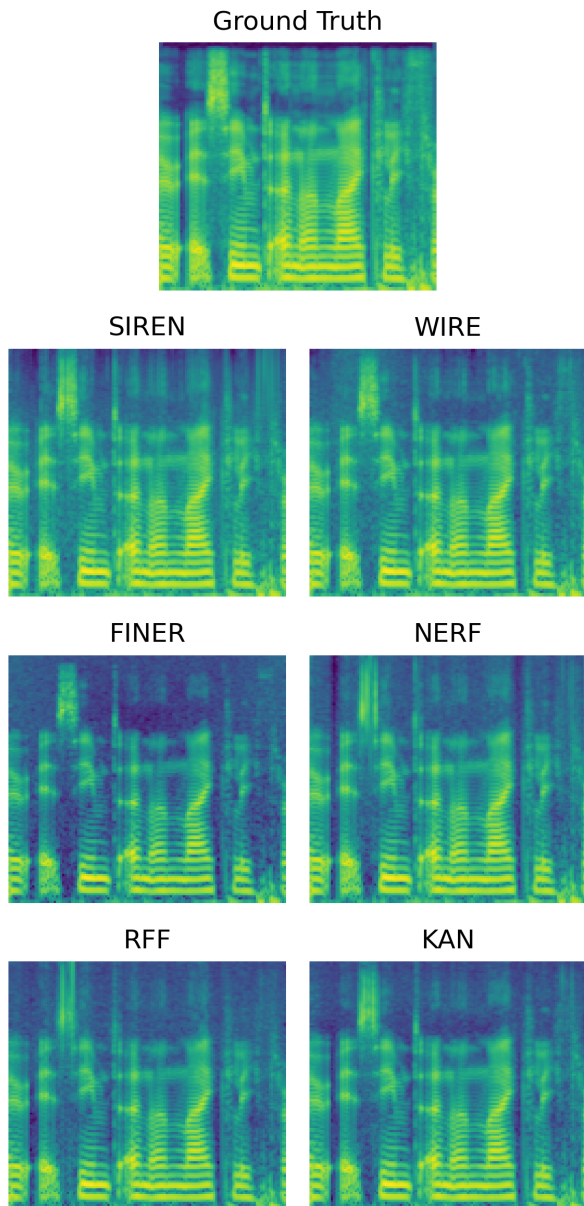


Figure 2: The comparison of spectrograms. We compare the original sample with the waveforms reconstructed using different INR approaches.

for audio signals, offering high reconstruction accuracy when integrated with hypernetwork-based architectures. By evaluating KANs against classical INR models like NeRF, FINER, WIRE, RFF, and SIREN, we highlight their potential as a foundational approach for efficient audio modeling, resulting in top-2 mean in 5 out of 7 considered quality metrics for 1.5 s audio, and top-2 in all 7 for 3 s audio. Additionally, by integrating KAN into hypernetwork frameworks like FewSound, performance improves significantly,

surpassing HyperSound with a 33.3% reduction in MSE, a 60.87% increase in SI-SNR, and an 8.66% in PESQ. The results suggest that KANs can serve as a powerful tool for audio representation, enabling adaptive processing across various datasets and tasks.

Since our experiments were conducted at a fixed sampling rate of 22,050 Hz, the impact of varying sampling strategies requires investigation in future work. Furthermore, integration with modern neural audio codecs and speech encoder systems presented in Tab 5 might be further expanded, in particular when investigating multilingual approach. The evaluation was restricted to English datasets due their prevalence. Additionally, the datasets lacked complex auditory scenarios, such as multi-speaker dialogues, emotional speech, and diverse acoustic scenes, which might be an interesting extensions to the research. It is important to note, that while KANs demonstrated efficiency in certain tasks, their computational demands may grow significantly for longer sequences or large-scale applications.

Future research should extend KAN-based models to multilingual datasets and diverse linguistic settings to enhance their generalization. Investigating the impact of sample length on performance could provide deeper insights into the balance between computational efficiency and fidelity. Architectural refinements may reduce resource requirements while maintaining accuracy, making KANs more scalable for practical deployment. Exploring their integration with multimodal frameworks, such as facial expressions or gestures, could enable advanced audio-visual synthesis and applications like avatar generation, an interesting path given hypernetworks already being used in visual modality (Przewiezlikowski et al., 2024; Kania et al., 2024). Additionally, developing interpretable models would improve transparency and understanding of KANs’ decision-making processes, which would increase trust in real-world applications and meeting legal requirements for practical usage. Finally, optimizing compatibility with a broader range of audio encoding systems could significantly enhance reconstruction quality, expanding the practical utility of KAN-based audio representations.



## References

- Batorski, P., Malarz, D., Przewiezlikowski, M., Mazur, M., Tadeja, S., and Spurek, P. Hyperplanes: Hypernetwork approach to rapid nerf adaptation. *arXiv preprint arXiv:2402.01524*, 2024.
- Chen, W.-Y., Liu, Y.-C., Kira, Z., Wang, Y.-C. F., and Huang, J.-B. A closer look at few-shot classification. In *International Conference on Learning Representations*, 2019.
- Chen, Z., Chen, Y., Liu, J., Xu, X., Goel, V., Wang, Z., Shi, H., and Wang, X. Videoinr: Learning video implicit neural representation for continuous space-time super-resolution. In *Proceedings of the IEEE/CVF Conference on Computer Vision and Pattern Recognition*, pp. 2047–2057, 2022.
- Chu, Y., Xu, J., Zhou, X., Yang, Q., Zhang, S., Yan, Z., Zhou, C., and Zhou, J. Qwen-audio: Advancing universal audio understanding via unified large-scale audio-language models. *arXiv preprint arXiv:2311.07919*, 2023.
- Collabora. WhisperSpeech GitHub repository, 2024. URL <https://github.com/collabora/WhisperSpeech>. [Online; accessed 3. Mar. 2024].
- Finn, C., Abbeel, P., and Levine, S. Model-agnostic meta-learning for fast adaptation of deep networks. In *International conference on machine learning*, pp. 1126–1135. PMLR, 2017.
- Gorji, A., Amrollahi, A., and Krause, A. A scalable walsh-hadamard regularizer to overcome the low-degree spectral bias of neural networks, 2023. URL <https://arxiv.org/abs/2305.09779>.
- Guo, H., Liu, C., Ishi, C. T., and Ishiguro, H. Using joint training speaker encoder with consistency loss to achieve cross-lingual voice conversion and expressive voice conversion. In *2023 IEEE Automatic Speech Recognition and Understanding Workshop (ASRU)*, pp. 1–8. IEEE, 2023.
- Ha, D., Dai, A., and Le, Q. V. Hypernetworks. *arXiv preprint arXiv:1609.09106*, 2016.
- Hu, E. J., Shen, Y., Wallis, P., Allen-Zhu, Z., Li, Y., Wang, S., Wang, L., and Chen, W. LoRA: Low-rank adaptation of large language models. In *International Conference on Learning Representations*, 2022. URL <https://openreview.net/forum?id=nZeVKeeFYf9>.
- Kania, A., Mihajlovic, M., Prokudin, S., Tabor, J., and Spurek, P. Fresh: Frequency shifting for accelerated neural representation learning, 2024. URL <https://arxiv.org/abs/2410.05050>.
- Kawa, P., Plata, M., Czuba, M., Szymański, P., and Syga, P. Improved deepfake detection using whisper features. In *INTERSPEECH 2023*, pp. 4009–4013, 2023. doi: 10.21437/Interspeech.2023-1537.
- Klocek, S., Maziarka, L., Wolczyk, M., Tabor, J., Nowak, J., and Smieja, M. Hypernetwork functional image representation. In *International Conference on Artificial Neural Networks*, pp. 496–510. Springer, 2019.
- Lanzendörfer, L. A. and Wattenhofer, R. Siamese SIREN: Audio compression with implicit neural representations. In *ICML 2023 Workshop Neural Compression: From Information Theory to Applications*, 2023. URL <https://openreview.net/forum?id=AgkMFYcOmM>.
- Liu, Z., Wang, Y., Vaidya, S., Ruehle, F., Halverson, J., Soljačić, M., Hou, T. Y., and Tegmark, M. Kan: Kolmogorov-arnold networks. *arXiv preprint arXiv:2404.19756*, 2024a.
- Liu, Z., Zhu, H., Zhang, Q., Fu, J., Deng, W., Ma, Z., Guo, Y., and Cao, X. Finer: Flexible spectral-bias tuning in implicit neural representation by variable-periodic activation functions. In *Proceedings of the IEEE/CVF Conference on Computer Vision and Pattern Recognition*, pp. 2713–2722, 2024b.
- Loshchilov, I. and Hutter, F. Decoupled weight decay regularization, 2019. URL <https://arxiv.org/abs/1711.05101>.
- Manocha, P., Jin, Z., Zhang, R., and Finkelstein, A. Cd-pam: Contrastive learning for perceptual audio similarity. *ICASSP, IEEE International Conference on Acoustics, Speech and Signal Processing - Proceedings*, 2021-June:196–200, 2021. ISSN 1520-6149. doi: 10.1109/ICASSP39728.2021.9413711. Publisher Copyright: © 2021 IEEE; 2021 IEEE International Conference on Acoustics, Speech, and Signal Processing, ICASSP 2021 ; Conference date: 06-06-2021 Through 11-06-2021.
- Mildenhall, B., Srinivasan, P. P., Tancik, M., Barron, J. T., Ramamoorthi, R., and Ng, R. Nerf: Representing scenes as neural radiance fields for view synthesis. In *ECCV*, 2020.
- Müller, T., Evans, A., Schied, C., and Keller, A. Instant neural graphics primitives with a multiresolution hash encoding. *ACM transactions on graphics (TOG)*, 41(4): 1–15, 2022.
- O’Reilly, P., Bugler, A., Bhandari, K., Morrison, M., and Pardo, B. Voiceblock: Privacy through real-time adversarial attacks with audio-to-audio models. In *Neural Information Processing Systems*, November 2022.

- Przewiezlikowski, M., Przybysz, P., Tabor, J., Zieba, M., and Spurek, P. Hypermaml: Few-shot adaptation of deep models with hypernetworks. *Neurocomputing*, 598:128179, 2024. ISSN 0925-2312.
- Radford, A., Kim, J. W., Xu, T., Brockman, G., McLeavey, C., and Sutskever, I. Robust speech recognition via large-scale weak supervision. In *International conference on machine learning*, pp. 28492–28518. PMLR, 2023.
- Rahaman, N., Baratin, A., Arpit, D., Draxler, F., Lin, M., Hamprecht, F. A., Bengio, Y., and Courville, A. On the spectral bias of neural networks, 2019. URL <https://arxiv.org/abs/1806.08734>.
- Rix, A., Beerends, J., Hollier, M., and Hekstra, A. Perceptual evaluation of speech quality (pesq)-a new method for speech quality assessment of telephone networks and codecs. In *2001 IEEE International Conference on Acoustics, Speech, and Signal Processing. Proceedings (Cat. No.01CH37221)*, volume 2, pp. 749–752 vol.2, 2001. doi: 10.1109/ICASSP.2001.941023.
- Saragadam, V., LeJeune, D., Tan, J., Balakrishnan, G., Veeraraghavan, A., and Baraniuk, R. G. WIRE: Wavelet Implicit Neural Representations, 2023. URL [https://openaccess.thecvf.com/content/CVPR2023/html/Saragadam\\_WIRE\\_Wavelet\\_Implicit\\_Neural\\_Representations\\_CVPR\\_2023\\_paper.html](https://openaccess.thecvf.com/content/CVPR2023/html/Saragadam_WIRE_Wavelet_Implicit_Neural_Representations_CVPR_2023_paper.html). [Online; accessed 3. Mar. 2024].
- Sheikh, A.-S., Rasul, K., Merentitis, A., and Bergmann, U. Stochastic maximum likelihood optimization via hypernetworks. *arXiv preprint arXiv:1712.01141*, 2017.
- Sitzmann, V., Martel, J., Bergman, A., Lindell, D., and Wetzstein, G. Implicit neural representations with periodic activation functions. In Larochelle, H., Ranzato, M., Hadsell, R., Balcan, M., and Lin, H. (eds.), *Advances in Neural Information Processing Systems*, volume 33, pp. 7462–7473. Curran Associates, Inc., 2020. URL [https://proceedings.neurips.cc/paper\\_files/paper/2020/file/53c04118df112c13a8c34b38343b9c10-Paper.pdf](https://proceedings.neurips.cc/paper_files/paper/2020/file/53c04118df112c13a8c34b38343b9c10-Paper.pdf).
- Siuzdak, H. SNAC: Multi-Scale Neural Audio Codec, 2024. URL <https://github.com/hubertsiuzdak/snac>. [Online; accessed 3. Dec. 2024].
- Smith, L. N. and Topin, N. Super-convergence: Very fast training of neural networks using large learning rates, 2018. URL <https://arxiv.org/abs/1708.07120>.
- Spurek, P., Winczowski, S., Tabor, J., Zamorski, M., Zieba, M., and Trzciński, T. Hypernetwork approach to generating point clouds. In *Proceedings of the 37th International Conference on Machine Learning*, pp. 9099–9108, 2020.
- Strümpler, Y., Postels, J., Yang, R., Gool, L. V., and Tombari, F. Implicit neural representations for image compression. In *ECCV*, 2022.
- Su, K., Chen, M., and Shlizerman, E. Inras: Implicit neural representation for audio scenes. In Koyejo, S., Mohamed, S., Agarwal, A., Belgrave, D., Cho, K., and Oh, A. (eds.), *Advances in Neural Information Processing Systems*, volume 35, pp. 8144–8158. Curran Associates, Inc., 2022.
- Szatkowski, F., Piczak, K. J., Spurek, P., Tabor, J., and Trzciński, T. Hypernetworks build implicit neural representations of sounds. In *Joint European Conference on Machine Learning and Knowledge Discovery in Databases*, pp. 661–676. Springer, 2023.
- Taal, C. H., Hendriks, R. C., Heusdens, R., and Jensen, J. A short-time objective intelligibility measure for time-frequency weighted noisy speech. In *2010 IEEE International Conference on Acoustics, Speech and Signal Processing*, pp. 4214–4217, 2010. doi: 10.1109/ICASSP.2010.5495701.
- Tancik, M., Srinivasan, P., Mildenhall, B., Fridovich-Keil, S., Raghavan, N., Singhal, U., Ramamoorthi, R., Barron, J., and Ng, R. Fourier features let networks learn high frequency functions in low dimensional domains. In Larochelle, H., Ranzato, M., Hadsell, R., Balcan, M., and Lin, H. (eds.), *Advances in Neural Information Processing Systems*, volume 33, pp. 7537–7547. Curran Associates, Inc., 2020. URL [https://proceedings.neurips.cc/paper\\_files/paper/2020/file/55053683268957697aa39fba6f231c68-Paper.pdf](https://proceedings.neurips.cc/paper_files/paper/2020/file/55053683268957697aa39fba6f231c68-Paper.pdf).
- Tancik, M., Mildenhall, B., Wang, T., Schmidt, D., Srinivasan, P. P., Barron, J. T., and Ng, R. Learned initializations for optimizing coordinate-based neural representations. In *Proceedings of the IEEE/CVF Conference on Computer Vision and Pattern Recognition*, pp. 2846–2855, 2021.
- Vaswani, A., Shazeer, N., Parmar, N., Uszkoreit, J., Jones, L., Gomez, A. N., Kaiser, L. u., and Polosukhin, I. Attention is all you need. In Guyon, I., Luxburg, U. V., Bengio, S., Wallach, H., Fergus, R., Vishwanathan, S., and Garnett, R. (eds.), *Advances in Neural Information Processing Systems*, volume 30. Curran Associates, Inc., 2017. URL [https://proceedings.neurips.cc/paper\\_files/paper/2017/file/](https://proceedings.neurips.cc/paper_files/paper/2017/file/)

[3f5ee243547dee91fbd053c1c4a845aa-Paper.pdf](#).

- Veaux, C., Yamagishi, J., and King, S. The voice bank corpus: Design, collection and data analysis of a large regional accent speech database. In *2013 International Conference Oriental COCOSDA held jointly with 2013 Conference on Asian Spoken Language Research and Evaluation (O-COCOSDA/CASLRE)*, pp. 1–4, 2013. doi: 10.1109/ICSDA.2013.6709856.
- Wang, Y., Yao, Q., Kwok, J. T., and Ni, L. M. Generalizing from a few examples: A survey on few-shot learning. *ACM computing surveys (csur)*, 53(3):1–34, 2020.
- Yamamoto, R., Song, E., and Kim, J.-M. Parallel wavegan: A fast waveform generation model based on generative adversarial networks with multi-resolution spectrogram. In *ICASSP 2020-2020 IEEE International Conference on Acoustics, Speech and Signal Processing (ICASSP)*, pp. 6199–6203. IEEE, 2020.
- Zeghidour, N., Luebs, A., Omran, A., Skoglund, J., and Tagliasacchi, M. Soundstream: An end-to-end neural audio codec. *IEEE/ACM Transactions on Audio, Speech, and Language Processing*, 30:495–507, 2021.

### A. Extended ablation study

At the beginning of this section we conclude the ablation study for 1.5 s audio samples by analyzing the influence of *learning rate*, *standalone scale spline* flag, *scale base* factor, *scale noise* factor and *scale spline* factor on KAN’s performance.

Table 10: Effect of various learning rate values on 1.5 s recordings

Learning rate	Num Params	MSE	PSNR	LSD	SI-SNR	PESQ	STOI	CDPAM
		→ 0	→ ∞	→ 0	→ 100	→ 4.5	→ 1	→ 0
0.01	31,080	<b>0.0007</b>	<b>40.5596</b>	1.3698	<b>19.4728</b>	3.2799	0.9877	0.1919
0.007	31,080	<b>0.0007</b>	40.5170	1.3284	19.3607	<b>3.3883</b>	0.9908	0.1927
0.006	31,080	<b>0.0007</b>	40.0159	1.3051	18.9209	3.3532	<b>0.9911</b>	<b>0.1770</b>
0.005	31,080	<b>0.0007</b>	40.0990	<b>1.2884</b>	18.9503	3.3588	0.9904	0.1913
0.001	31,080	0.0011	37.8920	1.3626	16.6339	2.5975	0.9711	0.2314

Table 10 shows the comparison of *learning rates*. Generally, KAN performs well and stably with higher learning rate setting. A learning rate of 0.001 yields the worst scores across all entries in the table. A learning rate of 0.01 achieves the best results in the PSNR and Si-SNR metrics, which are quantitative, while a learning rate near 0.006 produces the highest perceptual scores.

Table 11 shows the comparison of performance of KAN depending on whether the *enable scale spline* flag is set to False or True. The former results in skipping the theoretically redundant weights. However, it leads to a drop in all metric scores except MSE, with perceptual metrics being affected the most.

Table 11: Enable scale spline flag ablation for 1.5 s audio source

Enable Scale Spline	Num Params	MSE	PSNR	LSD	SI-SNR	PESQ	STOI	CDPAM
		→ 0	→ ∞	→ 0	→ 100	→ 4.5	→ 1	→ 0
False	28,860	<b>0.0007</b>	39.4067	1.5253	18.2321	2.7388	0.9653	0.2771
True	31,080	<b>0.0007</b>	<b>40.0990</b>	<b>1.2884</b>	<b>18.9503</b>	<b>3.3588</b>	<b>0.9904</b>	<b>0.1913</b>

At the end of this paragraph, we consider hyperparameters related to KAN initialization. The weight matrices  $w_b$  and  $w_s$  are initialized according to Kaiming uniform schema - the values are drawn from  $\mathcal{U}(-k, k)$  distribution, where

$$k = \sqrt{\frac{6}{(1 + 5a^2) \cdot fan\_in}}$$

and  $a$  is equal to *scale base* or *scale spline* for  $w_b$  and  $w_s$  respectively. The  $c_i$ s parameters are initialized by sampling a noise from  $\mathcal{N}(0, \sigma^2)$  distribution, and solving an instance of the least squares problem, so that *spline*( $x$ ) for a certain  $x$  is as close to the sampled noise as possible. The *scale noise* parameter is the standard deviation  $\sigma$  of the noise distribution.

Tables 12 and 13 show the ablation results for *scale spline* and *scale base* parameters respectively. In case of the first one, 0.5 seems to be the most optimal choice with the highest score for all metrics excluding LSD, where optimal choice is 1, and STOI, where the difference between the best scores is negligible. In case of *scale spline* the choice of the best value varies between metrics. Table 14 shows the results for the study of *scale noise* hyperparameter, with the lowest tested value of 0.025 attaining the best results in most of the metrics.

Table 12: KAN performance on 1.5 s, with respect to the scale base values.

Scale Base	Num Params	MSE	PSNR	LSD	SI-SNR	PESQ	STOI	CDPAM
		→ 0	→ ∞	→ 0	→ 100	→ 4.5	→ 1	→ 0
0.25	31,080	0.0008	39.9112	1.3386	18.7366	3.3149	0.9888	<b>0.1872</b>
0.5	31,080	<b>0.0006</b>	<b>41.0193</b>	1.3111	<b>19.8693</b>	<b>3.4322</b>	0.9904	0.1875
1	31,080	<b>0.0006</b>	40.8162	<b>1.2895</b>	19.6861	3.3821	0.9900	0.1930
2	31,080	<b>0.0006</b>	40.5262	1.3129	19.4204	3.2141	<b>0.9906</b>	0.2013
4	31,080	0.0008	39.5773	1.3195	18.4513	3.2608	0.9876	0.2062



Table 13: KAN performance on 1.5 s, with respect to the scale spline values.

Scale Spline	Num Params	MSE	PSNR	LSD	SI-SNR	PESQ	STOI	CDPAM
		$\rightarrow 0$	$\rightarrow \infty$	$\rightarrow 0$	$\rightarrow 100$	$\rightarrow 4.5$	$\rightarrow 1$	$\rightarrow 0$
0.25	31,080	0.0006	40.6718	1.3196	19.5770	<b>3.5030</b>	<b>0.9917</b>	0.1932
0.5	31,080	<b>0.0005</b>	40.9010	1.3057	19.8454	3.4086	0.9915	0.1895
1	31,080	0.0007	40.5384	<b>1.2895</b>	19.4369	3.4281	0.9915	0.1872
2	31,080	0.0006	<b>41.5030</b>	1.2973	<b>20.3684</b>	3.3479	0.9914	<b>0.1815</b>
4	31,080	0.0006	40.8259	1.2981	19.7534	3.3932	0.9903	0.1887

Table 14: KAN performance on 1.5 s, with respect to the scale noise values.

KAN Scale Noise	Num Params	MSE	PSNR	LSD	SI-SNR	PESQ	STOI	CDPAM
		$\rightarrow 0$	$\rightarrow \infty$	$\rightarrow 0$	$\rightarrow 100$	$\rightarrow 4.5$	$\rightarrow 1$	$\rightarrow 0$
0.4	31,080	0.0007	40.9740	1.3010	19.8608	3.4433	0.9910	0.1896
0.2	31,080	0.0007	40.2776	1.2849	19.1855	3.4280	<b>0.9915</b>	<b>0.1796</b>
0.1	31,080	0.0007	40.5541	<b>1.2796</b>	19.4436	3.4576	0.9913	0.1897
0.05	31,080	0.0007	40.0844	1.2864	18.9432	3.4004	0.9909	0.1846
0.025	31,080	<b>0.0006</b>	<b>41.0045</b>	1.2878	<b>19.9189</b>	<b>3.4605</b>	0.9897	0.1825

**Performance analysis of KAN on 3 s sounds** Next, we present the ablation study for 3 s recordings, considering the same hyperparameters as used for the 1.5 s samples.

Table 15 shows the impact of different *encoding lengths* on 3 s utterances. The absolute performance is generally lower across all metrics in relation to 1.5 s samples, e.g. the best PESQ decreasing from 3.62 to 2.90 and the best SI-SNR decreasing from 25.97 to 17.17. The results are much less conclusive than in case of 1.5 s, where length 16 was clearly optimal across most metrics. However, the majority of metrics (MSE, PSNR, SI-SNR and PESQ, STOI) are the best for encoding lengths of 24 and 16 respectively.

Table 15: KAN performance on the 3 s samples, with respect to the encoding length.

Encoding Length	Num Params	MSE	PSNR	LSD	SI-SNR	PESQ	STOI	CDPAM
		$\rightarrow 0$	$\rightarrow \infty$	$\rightarrow 0$	$\rightarrow 100$	$\rightarrow 4.5$	$\rightarrow 1$	$\rightarrow 0$
2	23,016	0.0036	30.4569	3.3098	4.2598	1.2121	0.6627	0.4217
4	25,704	0.0011	35.4080	2.0309	10.3129	1.5506	0.8204	<b>0.2926</b>
8	31,080	0.0006	38.9270	<b>1.2706</b>	14.0260	2.4971	0.9689	0.3578
10	33,768	0.0006	39.3990	1.3152	14.5468	2.8272	0.9779	0.3795
12	36,456	0.0005	39.6602	1.3722	14.7926	2.7818	0.9799	0.3730
16	41,832	0.0004	40.7796	1.4383	15.9502	<b>2.9095</b>	<b>0.9820</b>	0.3516
24	52,584	<b>0.0003</b>	<b>41.9264</b>	1.6033	<b>17.1797</b>	2.8385	0.9816	0.3429

Table 16 shows how sizes and depths of hidden layers influence results on 3 s samples. Similarly to 1.5 s (Table 7) the best performance is achieved by the largest network composed of [96, 48, 24] layers. The performance, however does not improve with the increasing size as gradually as for 1.5 s samples.

Table 16: KAN results on 3 s samples in relation to different number and sizes of hidden layers.

Layer Sizes	Num Params	MSE	PSNR	LSD	SI-SNR	PESQ	STOI	CDPAM
		$\rightarrow 0$	$\rightarrow \infty$	$\rightarrow 0$	$\rightarrow 100$	$\rightarrow 4.5$	$\rightarrow 1$	$\rightarrow 0$
[24, 12, 6]	10,500	0.0007	37.5744	1.4904	12.6576	1.7192	0.8912	0.3229
[24, 24, 12, 6]	18,564	0.0006	38.4196	1.3828	13.5231	1.9078	0.9393	0.3847
[48, 12, 6]	19,908	0.0008	38.0106	1.3325	13.0259	2.1609	0.9384	0.3734
[48, 12, 12, 6]	21,924	0.0006	38.3097	1.3430	13.3983	2.1817	0.9517	0.3886
[48, 16, 8]	23,408	0.0007	38.2895	1.3119	13.3530	2.2985	0.9562	0.3756
[48, 24, 12]	31,080	0.0006	38.9270	1.2706	14.0260	2.4971	0.9689	0.3578
[96, 48, 24]	102,480	<b>0.0005</b>	<b>40.9599</b>	<b>1.1792</b>	<b>16.1224</b>	<b>3.5224</b>	<b>0.9898</b>	<b>0.1594</b>

In comparison to the 1.5 s case, where a *spline order* of size 3 is clearly the optimal hyperparameter setting, its advantage is less evident in Table 17. KAN with a spline order equal to 5 achieves higher PNSR and SI-SNR scores, without falling too much behind in PESQ and STOI columns.

Table 17: KAN effectiveness in terms of diverse spline order sizes and 3 s long input

Spline Order	Num Params	MSE	PSNR	LSD	SI-SNR	PESQ	STOI	CDPAM
		$\rightarrow 0$	$\rightarrow \infty$	$\rightarrow 0$	$\rightarrow 100$	$\rightarrow 4.5$	$\rightarrow 1$	$\rightarrow 0$
1	28,860	<b>0.0006</b>	38.5038	1.4711	13.6106	2.2903	0.9540	0.3299
2	31,080	<b>0.0006</b>	38.9270	1.2706	14.0260	2.4971	0.9689	0.3578
3	33,300	0.0008	38.6639	<b>1.2540</b>	13.6820	<b>2.5639</b>	<b>0.9704</b>	0.3578
5	37,740	<b>0.0006</b>	<b>39.0929</b>	1.2663	<b>14.1943</b>	2.4499	0.9661	<b>0.3376</b>
7	42,180	<b>0.0006</b>	38.8824	1.3175	13.9657	2.1987	0.9573	0.3378

In table 18, table 19 and table 20, which correspond respectively to the ablations of *grid size*, *learning rate*, and *enable scale spline* flag on 3 s speeches, we observe similar conclusions and tendencies as in the 1.5s scenario. Described in Table 9 (Sect. 4.2), and Tables 10, 11(Appendix A), respectively.

Table 18: KAN effectiveness in terms of diverse grid size and 3 s long input

Grid size	Num Params	MSE	PSNR	LSD	SI-SNR	PESQ	STOI	CDPAM
		$\rightarrow 0$	$\rightarrow \infty$	$\rightarrow 0$	$\rightarrow 100$	$\rightarrow 4.5$	$\rightarrow 1$	$\rightarrow 0$
1	11,100	0.0029	31.3359	2.0005	5.4555	1.3828	0.7652	0.3998
5	19,980	0.0007	38.1135	1.4668	13.2103	1.9651	0.9160	0.2399
10	31,080	0.0006	38.9270	<b>1.2706</b>	14.0260	2.4971	0.9689	0.3578
12	35,520	0.0005	39.4903	1.2745	14.6419	2.6706	0.9739	0.3204
17	<b>46,620</b>	<b>0.0006</b>	<b>39.7273</b>	1.3224	<b>14.8089</b>	<b>3.0683</b>	<b>0.9734</b>	<b>0.2646</b>

Table 19: Effect of various learning rate values on 3 s recordings

Learning rate	Num Params	MSE	PSNR	LSD	SI-SNR	PESQ	STOI	CDPAM
		$\rightarrow 0$	$\rightarrow \infty$	$\rightarrow 0$	$\rightarrow 100$	$\rightarrow 4.5$	$\rightarrow 1$	$\rightarrow 0$
0.01	31,080	<b>0.0006</b>	<b>39.4961</b>	1.3238	<b>14.6358</b>	2.5597	0.9692	0.3940
0.007	31,080	<b>0.0006</b>	39.2295	1.2804	14.3368	<b>2.5669</b>	<b>0.9707</b>	0.3685
0.006	31,080	<b>0.0006</b>	39.1037	1.2781	14.2218	2.5516	0.9700	0.3633
0.005	31,080	<b>0.0006</b>	38.9270	<b>1.2706</b>	14.0260	2.4971	0.9689	0.3578
0.001	31,080	0.0007	37.7570	1.4674	12.8016	1.9302	0.9261	<b>0.3020</b>

Table 20: Enable scale spline flag ablation for 3 s audio source

Enable Scale Spline	Num Params	MSE	PSNR	LSD	SI-SNR	PESQ	STOI	CDPAM
		$\rightarrow 0$	$\rightarrow \infty$	$\rightarrow 0$	$\rightarrow 100$	$\rightarrow 4.5$	$\rightarrow 1$	$\rightarrow 0$
False	28,860	0.0007	38.0986	1.4767	13.2310	2.1969	0.9360	0.4218
True	31,080	<b>0.0006</b>	<b>38.9270</b>	<b>1.2706</b>	<b>14.0260</b>	<b>2.4971</b>	<b>0.9689</b>	<b>0.3578</b>

Finally, in Tables 21, 22, and 23 one can notice that the *scale base* and the *scale spline* hyperparameters do not significantly influence the performance. While manipulating *scale base*, all metrics except for CDPAM vary by less than 9% (the mentioned CDPAM under 16%). Moreover, apart from MSE that almost does not change, the changes in metric scores are not monotonic with respect to the changes in parameter values.

Table 21: Evaluation of different scale base factors on 3 s audio samples

Scale Base	Num Params	MSE	PSNR	LSD	SI-SNR	PESQ	STOI	CDPAM
		$\rightarrow 0$	$\rightarrow \infty$	$\rightarrow 0$	$\rightarrow 100$	$\rightarrow 4.5$	$\rightarrow 1$	$\rightarrow 0$
0.25	31,080	0.0006	39.0743	1.2804	14.1621	2.4855	0.9654	0.3574
0.5	31,080	0.0006	39.1813	1.2744	14.2891	<b>2.5813</b>	<b>0.9714</b>	<b>0.3485</b>
1	31,080	0.0006	38.9647	<b>1.2643</b>	14.0714	2.5415	0.9693	0.3573
2	31,080	0.0006	38.8621	1.2980	13.9575	2.5120	0.9654	0.3932
4	31,080	<b>0.0005</b>	<b>39.7455</b>	1.3119	<b>14.9256</b>	2.3783	0.9612	0.4040

Table 22: Evaluation of different scale spline factors on 3 s audio samples

Scale Spline	Num Params	MSE	PSNR	LSD	SI-SNR	PESQ	STOI	CDPAM
		$\rightarrow 0$	$\rightarrow \infty$	$\rightarrow 0$	$\rightarrow 100$	$\rightarrow 4.5$	$\rightarrow 1$	$\rightarrow 0$
0.25	31,080	<b>0.0006</b>	<b>39.3700</b>	1.2761	<b>14.4961</b>	<b>2.6388</b>	<b>0.9713</b>	0.3758
0.5	31,080	<b>0.0006</b>	38.9780	1.2698	14.0723	2.5493	0.9689	0.3678
1	31,080	<b>0.0006</b>	39.0889	<b>1.2654</b>	14.2169	2.4618	0.9643	0.3667
2	31,080	<b>0.0006</b>	38.9006	1.2735	13.9963	2.5288	0.9696	0.3663
4	31,080	<b>0.0006</b>	38.9421	1.2740	14.0168	2.4376	0.9666	<b>0.3448</b>

Table 23: Evaluation of different scale noise factors on 3 s audio samples

Scale Noise	Num Params	MSE	PSNR	LSD	SI-SNR	PESQ	STOI	CDPAM
		$\rightarrow 0$	$\rightarrow \infty$	$\rightarrow 0$	$\rightarrow 100$	$\rightarrow 4.5$	$\rightarrow 1$	$\rightarrow 0$
0.4	31,080	<b>0.0006</b>	39.0755	1.2712	14.1628	2.5252	0.9659	0.3711
0.2	31,080	<b>0.0006</b>	<b>39.1540</b>	1.2631	<b>14.2794</b>	<b>2.5684</b>	0.9687	0.3604
0.1	31,080	<b>0.0006</b>	39.0749	<b>1.2624</b>	14.1858	2.5053	<b>0.9698</b>	<b>0.3488</b>
0.05	31,080	<b>0.0006</b>	39.0345	1.2699	14.1197	2.5075	0.9680	0.3601
0.025	31,080	<b>0.0006</b>	39.1100	1.2706	14.2064	2.5701	0.9679	0.3613